scientific reports

Check for updates

OPEN

Experimental study on dynamic mechanical properties of multidirectional constrained water-bearing coal samples under dynamic-static coupling loading

Beijing Xie[1], Ben Zhang[1]✉, Shunkun Zhao[2] & Shanyang Wei[2]

The objective of this study is to investigate the dynamic mechanical properties of coal and rock under deep water conditions. The research employs an enhanced Split Hopkinson Pressure Bar (SHPB) testing system. Five sets of dynamic impact experiments were conducted on coal samples under varying loading conditions to analyse the changes in dynamic strength, energy dissipation, fractal dimension and other characteristics of coal samples under different water content states were analyzed. The experimental results demonstrate that: (1) Under specific strain rate conditions, the dynamic strength of saturated coal samples is lower than that of natural coal samples. As the strain rate gradually increases, the bonding force generated by free water and the Stefan effect jointly act, and the peak strength of saturated coal samples under high strain rate loading conditions is higher than that of natural coal samples. (2) Under certain strain rate conditions, the absorption energy of saturated coal samples is approximately 10% to30% lower than that of natural coal samples, and deformation hysteresis phenomenon occurs in natural coal samples, thereby improving the dynamic strength of natural coal samples relative to saturated coal samples; (3) The fractal dimension of saturated coal samples with a specific strain rate under three-dimensional dynamic static combination loading is higher than that of natural coal samples, and the percentage of small particle coal samples with debris is higher than that of natural coal samples; Finally, based on the HJC model, some coal samples were selected to simulate the coal rock failure characteristics during the triaxial loading process using ANSYS/LS-DYNA, and their stress–strain curves and failure morphology diagrams were obtained. The discrepancy between the numerical simulation and the experimental results was less than 10%, thereby further elucidating and corroborating the coal failure process and dynamic mechanical characteristics.

Keywords Water-bearing coal rocks, Dynamic mechanical properties, Dynamic and static coupling loading, SHPB, Energy dissipation, Fractal theory

As a primary energy source, coal plays a significant role in the global energy economy. As economies continue to develop, countries around the world are increasing their exploitation of primary energy sources, including coal, oil, natural gas, and other primary energy sources. The long-term mining of mineral resources and energy will inevitably lead to the depletion of shallow resources. Consequently, the exploitation of deep mineral resources and energy will become an inevitable trend. In underground coal mining engineering, mechanical strength of the coal body, which constitutes the main self-supporting structure, is subject to significant influence from a number of factors, including water content and the impact of excavation activities such as drilling and blasting.

[1]School of Emergency Management and Safety Engineering, China University of Mining and Technology, Beijing 100083, China. [2]School of Mining, Guizhou University, Guiyang 550025, China. ✉email: BQT2210103031@student.cumtb.edu.cn

The combined effect of dynamic and static loads can result in a range of geological disasters, including coal rock deformation, tunnel or mine water inrush, and rock burst are caused[1–5]. Therefore, a comprehensive understanding of the dynamic mechanical response of coal under different hydrological conditions is of great guiding significance for the safety design and evaluation of deep coal mining engineering.

Therefore, a considerable body of research has been conducted by numerous scholars on the dynamic mechanical properties of coal and rock in a variety of occurrence conditions. In 1949, Kolsky invented the Split Hopkinson Pressure Bar (SHPB) with the aim of exploring the mechanical properties of materials under impact loads. Since then, it has been widely used in the study of the mechanical properties of concrete[6], soil, steel[7], and other composite materials[8–10] under different strain rates and loading conditions. The International Society for Rock Mechanics (ISRM) proposed dynamic testing methods for uniaxial compression[11] and triaxial compression[12] using coal rock dynamic compression as an example. Many researchers have made targeted improvements to SHPB based on their own needs. Li et al.[13] and Gong et al.[14] developed active confining and axial compression devices on the basis of traditional SHPB devices, and initially achieved dynamic static joint loading. Yin et al.[15] added a temperature control device to SHPB and analyzed the dynamic mechanical properties of rocks under the coupling effect of temperature and pressure. However, the above experimental setup still used the conventional uniaxial compression SHPB system was still used.

In general, coal rock often undergoes chemical and physical interactions with water,which result in alterations to the mechanical properties of the rock[16–19]. In light of the above, numerous scholars have conducted comprehensive research into the mechanical response of coal and rock with varying water contents. This has involved the use of a separated Hopkinson compression rod to conduct uniaxial compression tests on a range of materials, including sandstone, limestone, granite, and coal[20–26], as well as Brazilian splitting tests[27,28]. The experimental results show that the mechanical properties of various rock materials, such as compressive strength, tensile strength, fractal dimension, shear strength, and Young's modulus, exhibit varying degrees of weakening with the increasing of water content, and the occurrence of this weakening phenomenon is directly proportional to the clay content in the rock[29–32]. However, in engineering practice, engineering disturbances such as blasting, roof collapse, and mechanical vibration are often encountered, resulting in a stress state of dynamic and static coupling of coal and rock. A plethora of research findings have demonstrated that the dynamic and static coupled loading of coal and rock exhibits notable strain rate and confining pressure effects on the dynamic mechanical characteristics of rock materials. This is evidenced by the observation that the dynamic peak strength, elastic modulus, absorbed energy, and other dynamic parameters of rock increase with the rise in strain rate and confining pressure[33–35]. It should be noted that this statement only applies to natural coal samples and that the applicability to saturated coal samples is not yet clear. Furthermore, as the depth of mining increases, the composition and structure of the geostress on deep coal and rock will undergo changes. It is therefore essential to consider not only the influence of high confining pressure on the dynamic mechanical properties of deep coal and rock, but also the initial factor of axial pre-stressed stress when studying the dynamic mechanical properties of deep coal and rock. It is valuable to study the dynamic mechanical response of fully saturated coal samples under dynamic static coupling loading and explore the underlying mechanisms based on this study. In the following chapters, the experimental scheme is first introduced, and then, based on the SHPB test results, the dynamic characteristics, energy dissipation laws, failure characteristics, and fractal laws of coal samples under natural and saturated states are discussed. This allowed for an analysis and discussion of the mechanism of the Stefan effect and the bonding force of free water, as well as an explanation of the experimental results.

Experimental materials and methods

Sample preparation

The coal samples employed in the experiments were obtained from the 1268.3 m 19# seam 221,908 backing face, situated at a distance of 42 m from the upper exit of the Shanjiaoshu Coal Mine in Guizhou Province, China. The coal samples were drilled and polished to a height of 30 mm, a diameter of 50 mm, and a non-parallelism of < 0.02 mm between the two end faces, in accordance with the International Society for Rock Mechanics (ISRM) standard for rock dynamics testing. To ensure homogeneity, all coal samples were taken from the same coal seam and underwent a longitudinal wave velocity test prior to the commencement of the experiment. Subsequently, the coal samples were divided into five groups one coal sample from each group was saturated with water. Following a period of 96 h during which the coal samples were permitted to absorb water naturally in a water tank, the samples were weighed at regular intervals until the weight remained relatively constant, which was deemed to be indicative of saturation. The procedure is illustrated in Fig. 1. Subsequent to the water saturation treatment, the fundamental physical parameters of the coal samples were quantified, and the findings are presented in Table 1.

Test equipment and scheme

This experiment uses the Hopkinson rod (SHPB) triaxial dynamic and static combination test system of the Safety Laboratory of China University of Mining and Technology (Beijing). The test system is capable of increasing the circumferential active circumferential pressure and axial pre-stress compared with the conventional Hopkinson rod test system, and the bullets, incident rods, and reflector rods of the device are made of alloy steel, with lengths of 400 mm, 3000 mm, and 2500 mm, and diameters of 50 mm, modulus of elasticity of 206GPa, density of 7.74 g/cm^3, and longitudinal wave propagation velocity of 5159 m/s. The strain signals were subsequently processed and calculated in order to obtain the signals of a typical sample, utilising an ultra-dynamic strain collector (LK2019A) and a data processing system. This is illustrated in Fig. 2b. Furthermore, Fig. 2a and c illustrate the schematic diagram of the test setup and the physical diagram of the test setup, respectively.

The acquired coal samples were divided into two groups, namely the saturated state and natural state, and numbered S1 ~ S5 and N1 ~ N5. The samples S1-S3 and N1-N3 were subjected to a test peripheral and axial

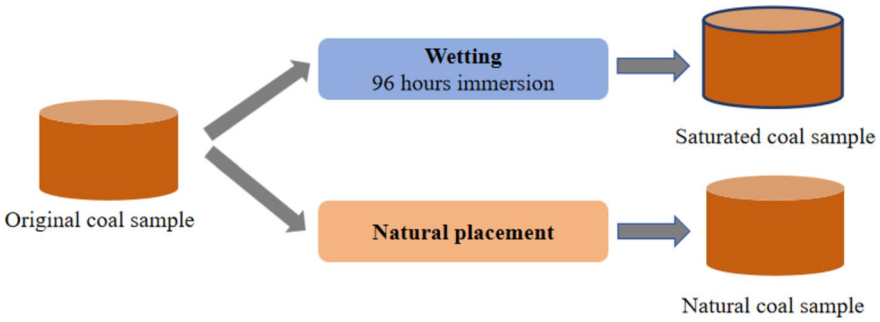

Figure 1. Coal sample preparation process diagram.

Water content	Coal sample number	Quality/(g)	Height/(mm)	Diameter/(mm)	Longitudinal wave/ ($m \cdot s^{-1}$)	Quality after soaking in water/(g)	Longitudinal waves after soaking in water/($m \cdot s^{-1}$)
Natural state	N_1	86.900	29.54	49.40	2.03	/	/
	N_2	89.276	29.97	49.44	1.99	/	/
	N_3	93.611	30.02	49.46	1.96	/	/
	N_4	90.789	29.99	49.41	2.27	/	/
	N_5	91.035	29.86	49.46	1.97	/	/
Saturated	S_1	90.338	30.17	49.42	2.03	91.395	1.76
	S_2	84.181	30.23	49.47	2.08	85.158	1.97
	S_3	91.089	30.12	49.44	1.94	92.422	2.06
	S_4	86.950	29.85	49.44	2.27	86.939	1.92
	S_5	88.560	30.17	49.43	1.97	89.675	1.72

Table 1. Basic physical parameters of coal sample.

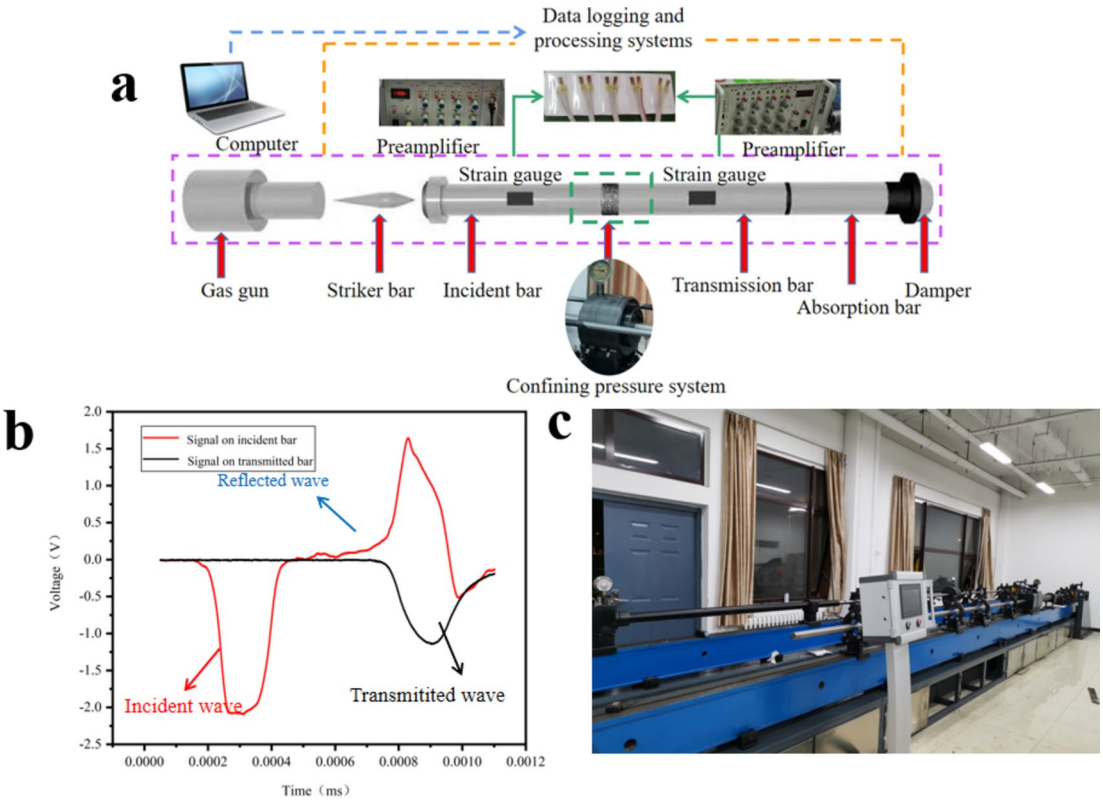

Figure 2. SPHB test equipment and principle: (**a**) schematic diagram; (**b**) Signals collected by the strain gauge; (**c**) Physical drawings.

pressure of 4 MPa, while the samples S4 and N4 were subjected to a test peripheral and axial pressure of 8 MPa. Finally, the samples S5 and N5 were subjected to a test peripheral and axial pressure of 12 MPa. This was done in order to achieve a loading of the coal samples with different strains.It should be noted that the impact velocity and strain rate are linearly related (as shown in Fig. 3). The impact velocities of natural state coal samples N1-N5 were 7.648 m/s, 10.708 m/s, 14.53 m/s, 10.948 m/s, 10.681 m/s, and the impact velocities of saturated state coal samples S1-S5 were 7.777 m/s, 10.622 m/s, 14.823 m/s, respectively, 9.338 m/s, 10.445 m/s.

Analysis of three-dimensional dynamic-static combination SHPB test results

Strength properties

The test enables the calculation of dynamic mechanical parameters of coal samples under different loading conditions, as illustrated in Table 2.

The stress–strain diagrams of coal samples in the saturated state and natural state can be obtained by processing the experimental data, as illustrated in Fig. Figure 4a,b illustrates that the stress–strain curves in the saturated state and natural state exhibit a comparable trend. In the initial stage, the peripheral and axial pressures of the three-dimensional impact test result in compaction of the coal sample upon application of the impact power. Consequently, coal samples subjected to three-dimensional dynamic and static combined loading do not experience a compaction stage, directly entering the elastic deformation stage. This contrasts with the results of the uniaxial impact test. Subsequently, the coal samples enter the plastic deformation stage. During this stage, the old cracks remain relatively stable in terms of expansion, while the new cracks continue to increase in size. As the strain continues to increase, the stress reaches its peak, which is known as the dynamic compressive strength. At this point, due to the coal rock's multi-porous nature, the coal rock specimen will not be immediately destroyed, as it still possesses a certain load-bearing capacity. Subsequently, it enters the unloading stage, and the cracks continue to expand until the specimen is destroyed.

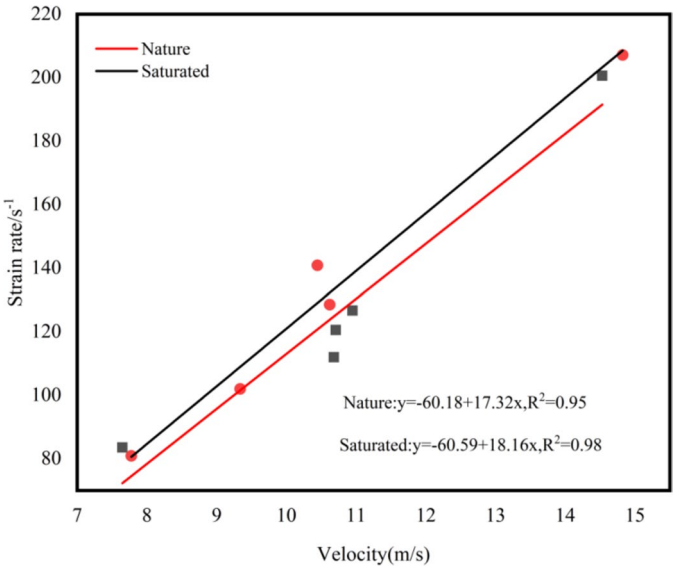

Figure 3. Relation between strain rate and impact velocity.

Water content	Coal sample number	Hydrostatic pressure/(MPa)	Confining pressure/(MPa)	Impact velocity/(m/s)	Average strain rate/(s^{-1})	Peak intensity/(MPa)
Natural state	N_1	4	4	7.648	83.5511	60.145
	N_2	4	4	10.708	120.5779	89.527
	N_3	4	4	14.530	200.5974	130.346
	N_4	8	8	10.948	126.6930	80.781
	N_5	12	12	10.681	111.9797	113.459
Saturated	S_1	4	4	7.777	80.9080	58.494
	S_2	4	4	10.622	128.5653	84.136
	S_3	4	4	14.823	207.1237	134.055
	S_4	8	8	9.338	102.0034	75.809
	S_5	12	12	10.445	140.8780	89.871

Table 2. Dynamic mechanical parameters of coal samples.

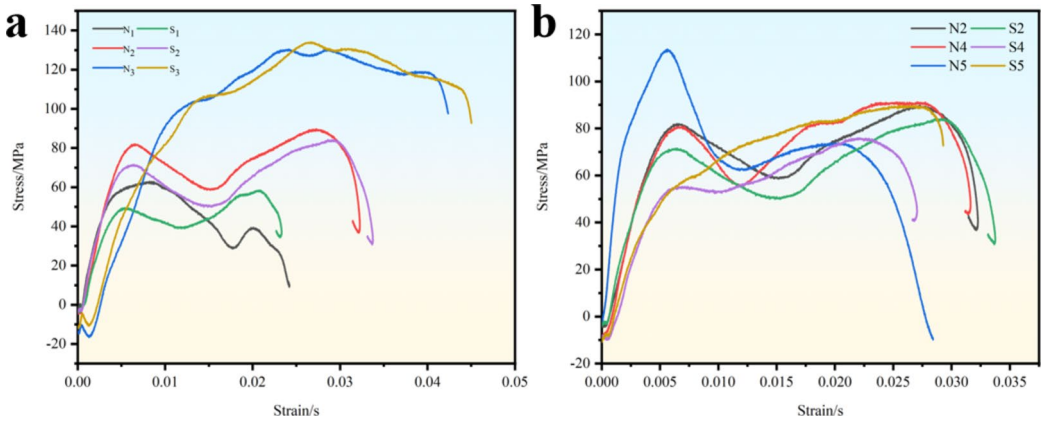

Figure 4. Stress–strain curve (**a**) same confining pressure with different axial pressures (**b**) same confining pressure with different axial pressures.

It is worth noting that in Fig. 4a, the peak stresses of the saturated coal samples in the first and second groups are smaller than that of the natural coal samples, while in the third group, the peak stresses of the saturated coal samples are slightly higher than that of the natural coal samples due to the increase of strain rate, which is consistent with the results of the study done by Xin Cai[36] and others, who believed that the weakening effect of water on the strength of coal rock is gradually diminished with the increase of the strain rate, and even at a certain critical strain rate, water can enhance the dynamic mechanical properties of coal rock. It can be demonstrated that water can enhance the dynamic mechanical properties of coal rock. This phenomenon can be attributed to the combined effect of the bonding force generated by free water and the Stefan effect work, which impedes the expansion of coal rock fissures, thereby enhancing the strength of the coal rock[37]. In Fig. 4b, there is no similar situation, but in the same strain rate range, the dynamic peak compressive strength of the coal samples increased significantly when the peripheral and axial pressures became 12 MP, and the dynamic peak strength of the natural coal samples was greater than that of the saturated coal samples under a certain strain rate, and water saturation weakened the compressive strength of the coal samples, whereas an increase in the peripheral pressure would enhance the dynamic peak compressive strength of the coal samples. Concurrently, the double peak phenomenon manifests in disparate strain rates, peripheral and axial pressures, and the curves exhibit a discernible leap. This phenomenon may be attributed to the role of charcoal in micro-breakage of crystals, a conclusion corroborated by numerous scholars[38–40], his phenomenon can be described as follows: the stress reaches the first dynamic stress peak (compressive strength), and with the increase of the strain, the stress is then decreased and the coal rock specimen enters the yielding stage, as the stress increases again, the stress reaches the second peak maximum value coal rock begins to break.

As the strain rate is increased, the peak stress the coal samples also rises gradually. The peak stresses of the natural coal samples (N1-N5) are 60.145 MPa, 89.527 MPa, 130.346 MPa, 80.781 MPa, and 113.459 MPa respectively. The saturated coal samples (S1-S5) exhibit peak stresses of 58.494 MPa, 84.136 MPa, 134.055 MPa, 75.809 MPa, and 89.871 MPa, respectively. and the relative errors between them are shown in Fig. 5b, corresponding to the saturated coal samples, 134.055 MPa, 75.809 MPa, 89.871 MPa, and the relative error between them is shown in Fig. 5b, corresponding to the natural coal samples, the dynamic triaxial compressive strength of the

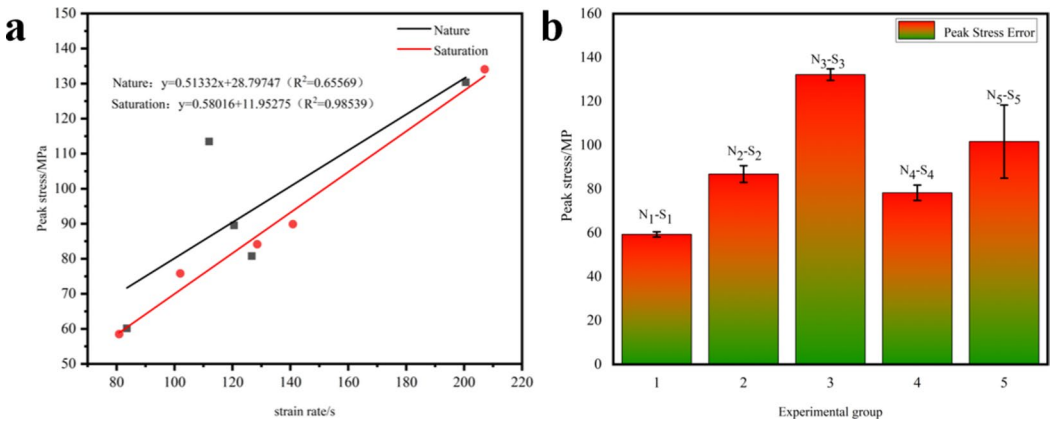

Figure 5. Plot of peak stress relationship (**a**) strain rate vs. peak stress; (**b**) error plot of peak stress in the same group.

saturated coal samples compared to the natural state decreased (Groups 1, 2, 4, and 5) by 2.82%, 6.02%, 6.15%, and 20.78% increased (Group 3) by about 2.85%. The weakening effect of group 5 is more obvious, which may be because the state of high perimeter pressure reduces the fracture strength factor of the internal cracks in the coal rock, changes the stress field at the crack tip and thus inhibits the rupture of the coal samples. From Fig. 5a, it can be observed that the peak stresses in the saturated state exhibit a strong linear relationship with the increase in strain rate, while the dynamic peak stresses in the natural coal samples under the state of high circumferential pressure exhibit a significant increase. Furthermore, the peak stresses under the remaining loading conditions also exhibit a strong linear relationship with the increase in strain rate.

Energy consumption analysis of coal samples

The destruction of a coal rock body is essentially a process of energy release and dissipation within the rock body, which contains three processes energy absorption, conversion and release. In practical engineering applications, the absorption energy of coal rock crushing can be used to indicate the degree of difficulty of coal rock destruction. The absorption energy W_d of coal rock specimen can be calculated by the following formula[41]:

$$W_d = W_i - (W_r + W_t) \tag{1}$$

where: W_d, W_i, W_r and Wt are the absorbed, incident, reflected and transmitted energy, respectively, and the above parameters can be obtained by the following equations:

$$W_i = E_0 C_0 A_0 \int_0^t \varepsilon_i^2(t)dt \tag{2}$$

$$W_r = E_0 C_0 A_0 \int_0^t \varepsilon_r^2(t)dt \tag{3}$$

$$W_t = E_0 C_0 A_0 \int_0^t \varepsilon_t^2(t)dt \tag{4}$$

where: E_0 is the modulus of elasticity of the incident and transmitted rods, C_0 is the propagation speed of the stress wave in the rod, A_0 is the cross-sectional area of the incident and transmitted rods, ε_i, ε_r and ε_t are the incident strain, the reflected strain and the transmitted strain at a certain moment, respectively, and in the elastic phase, the speed of the stress wave, C_e; it can be expressed by using the density ρ_e and the modulus of elasticity of the Hopkinson rods, $C_e = \sqrt{E_e/\rho_e}$, for this Hopkinson compression rod test system, $C_e = 5159$ m/s. The calculation of each energy parameter is shown in Table 3.

The energy parameters in Table 3 are plotted statistically and analytically to obtain Fig. 6, through which demonstrates that the incident energy increases with the increase of strain rate under the same circumferential axial pressure. It is noteworthy that, similar to the strength characteristics, the incident energy of saturated coal samples is lower than that of natural coal samples in the case of low strain rate, while the weakening effect component decreases with the increase of strain rate, and the bonding force generated by the free water of water-saturated coal samples under the action of high strain rate and the Stefan effect work together to impede the expansion of the coal-rock fissures, thus enhancing the incident energy. Furthermore, the phenomenon of increasing the incident energy with the increase of the surrounding pressure was observed under varying axial pressure conditions. This may be attributed to the limiting effect of the surrounding pressure on the transverse deformation of the coal samples during the force application, thereby enhancing the compressive strength of the coal and improving the incident energy.

The absorbed energy of each group of coal samples is obtained by calculating the energy consumption of each group of coal samples.This calculation determines the energy required for the destruction of coal samples to some extent. Figure 7 illustrates that, with the exception of the third group of saturated coal samples, the absorbed

Water content	Coal sample number	Incident energy/J	Reflectance energy/J	Transmittance energy/J	Absorptive energy/J
Natural state	N_1	125.05270	52.53800	25.83000	46.68470
	N_2	197.94550	80.27150	59.78060	57.89340
	N_3	375.52500	228.07800	92.52600	54.92100
	N_4	234.75680	103.86100	70.23535	60.66045
	N_5	226.15970	114.90600	62.59220	48.66150
Saturated	S_1	122.71467	54.77869	34.66160	33.27438
	S_2	195.15440	91.88910	54.18810	49.07720
	S_3	412.39880	252.02870	100.34267	60.02743
	S_4	178.53833	75.21370	47.99920	55.32543
	S_5	180.60260	91.27700	54.97100	34.35460

Table 3. Energy parameters of coal sample.

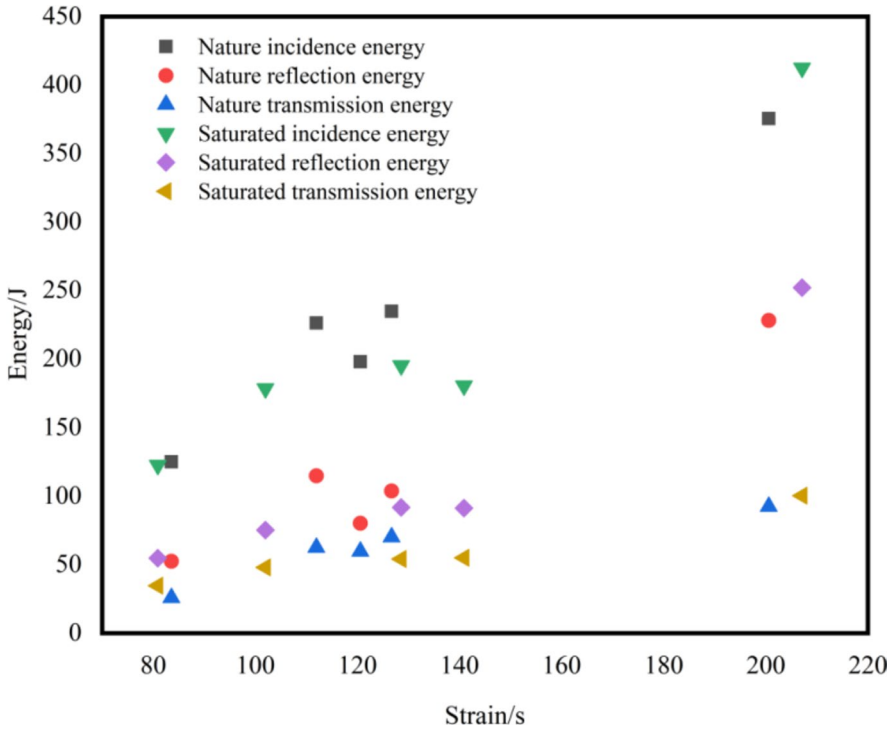

Figure 6. Relation between strain rate and incident energy, reflected energy and absorbed energy.

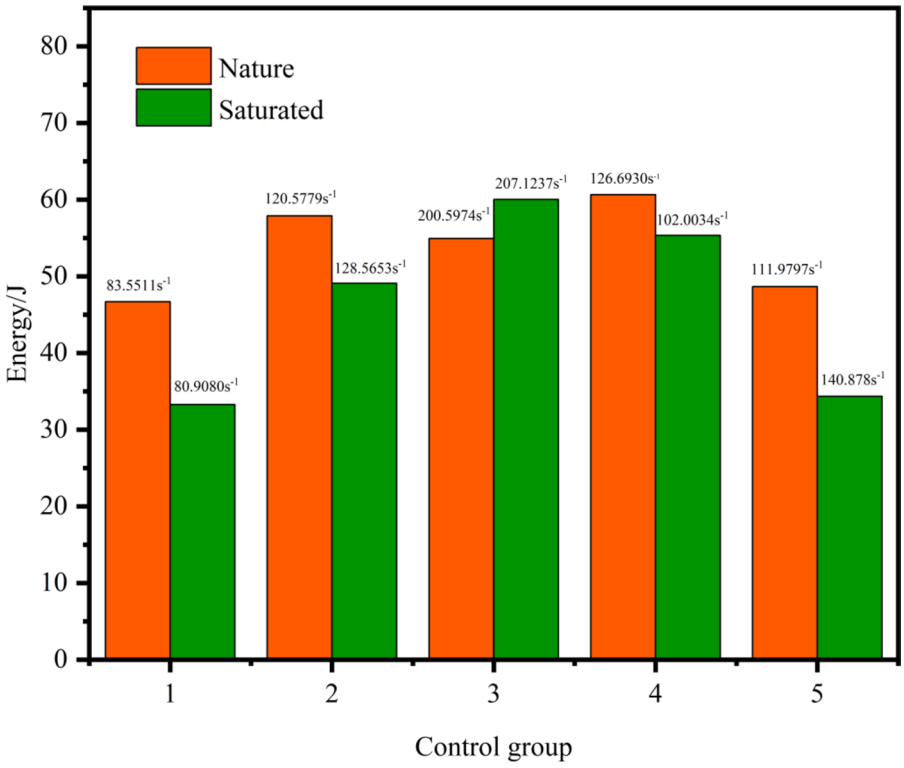

Figure 7. Absorption energy error diagram of the same group.

energy is larger than that of natural coal samples.Furthermore, and the absorbed energy of the saturated coal samples is smaller than that of the natural coal samples under the same strain rate. This is accompanied by a deformation hysteresis phenomenon occurs in the specimen as the absorbed energy in the specimen increases, which enhances the dynamic strength of the coal samples. This indicates that the energy required for the destruction of coal samples in a saturated state under low strain rate conditions is lower than that in a natural coal samples. This suggests that water saturation has a certain degree of weakening effect on coal samples.

Damage patterns and fractal characteristics

The crushing effect of coal samples under three-dimensional dynamic and static combined loading reflects the force state of coal samples, and by the characteristics of fractal theory, the crushing block size distribution can be used to evaluate the crushing effect of coal rock, and in the previous studies, the statistical function of crushing block size distribution is relatively widely used with R-R (Rosin–Rammler) distribution and G-G-S (Gate-Gaudin-Schuhmann) distribution[42–44] widely used. In this paper, the G-G-S distribution function is used to fracture the coal samples into dimensions. It is obtained from the literature[45]:

$$\alpha=\frac{\lg(m_r/m)}{\lg r} \tag{5}$$

where: m_r is the mass of the fragment whose particle size is smaller than r, and m is the total mass of the sample fragment.

$$D=3-\alpha \tag{6}$$

where: m_r is the mass of fragments with particle size less than r,m is the total mass of the sample fragments.

The tested crushed coal samples were sieved by round hole coal sieves with diameters of 30 mm, 20 mm, 10 mm, 3 mm, 2 mm and 1 mm respectively, and the coal samples with diameters below each level were weighed, and the results of the sieving were shown in Fig. 8, and then the fractal dimensions of the coal samples under different conditions could be calculated by the formulae (5) ~ (6), as shown in Table 4.

The lg(mr/m) and lgr curves of natural and saturated coal samples under different loading conditions are shown in Figs. 9 and 10, from which it can be seen that except for the first group of coal samples with a loading rate of 4 m/s which did not undergo fragmentation, the remaining four groups of coal samples showed obvious changes in the pattern of the fractal rule of the particle-size-mass fractal characteristics. The slope α of the curves of natural and saturated coal samples under the same axial pressure and circumferential pressure conditions increases with the increase of loading rate, in other words, with the increase of loading rate, the mass percentage of coal chips corresponding to the low particle size gradually increases, and the mass percentage of coal chips corresponding to the high particle size gradually decreases. It is noteworthy that the loading strain rate in the third group exhibited a notable increase, which resulted in the formation of a bonding force between the free water of water-filled coal samples and the Stefan effect under the influence of high strain rates. This prevented the expansion of coal rock fissures, leading to a reduction in the curve slope α in comparison to natural coal samples. Conversely, under conditions of varying peripheral axial pressures, the increase in peripheral pressures constrained the extent of transverse damage, reducing the fragmentation of the samples. This resulted in an increase in the slope α. Consequently, the slope α is observed to increase. In general, the slope of the saturated coal samples is greater than that of the natural coal samples under low strain rate loading conditions, which suggests that the coal samples are subjected to more intense crushing under saturated conditions.

The change rule of the fractal dimension of natural and saturated coal samples with loading rate is illustrated in Fig. 11. The fractal dimension of natural and saturated coal samples decreases with the increase of loading rate, indicating a reduction in the degree of fragmentation of coal samples. In the case of a lower strain rate, the fractal dimension of saturated coal samples is slightly larger than that of natural coal samples. This indicates that the presence of water weakens the integrity and stability of the microfracture structure of the coal samples, and that the microfractures are more easily broken under the action of external force. This is macroscopically manifested in the reduction of the strength of water-containing coal samples and the increased degree of fragmentation. As evidenced by the outcomes of the third experimental group, an increase in the strain rate to a specific threshold can enhance the strength of coal samples through the action of bonding forces and the Stefan effect in saturated water conditions.

SHPB numerical simulation analysis

In the above experiment, we systematically described the failure process of coal rock mass based on experimental results. However, the dynamic characteristics and crack evolution laws of coal rock specimens under impact loads are extremely complex, and there are significant differences between the dynamic characteristics and crack evolution laws under quasi-static loads. In this case, the impact response of heterogeneous materials (such as coal and rock) is usually determined by comparing laboratory experiments and numerical simulations. In this section, we utilise the LS-DYNA program to simulate the impact of coal and rock specimens in accordance with the HJC model. This enables us to compare the simulated crack evolution process and peak strength with experimental test results, thereby revealing the overall process and internal mechanism of sample failure.

Establishment of numerical simulation models

A model of the Hopkinson bar (SHPB) triaxial dynamic static combination test system of the Safety Laboratory of China University of Mining and Technology (Beijing) was modeled and constructed with the same dimensions based on ANSYS/LS-DYNA.. The dimensions of the model were as follows: bullet, 400 mm; incident bar,

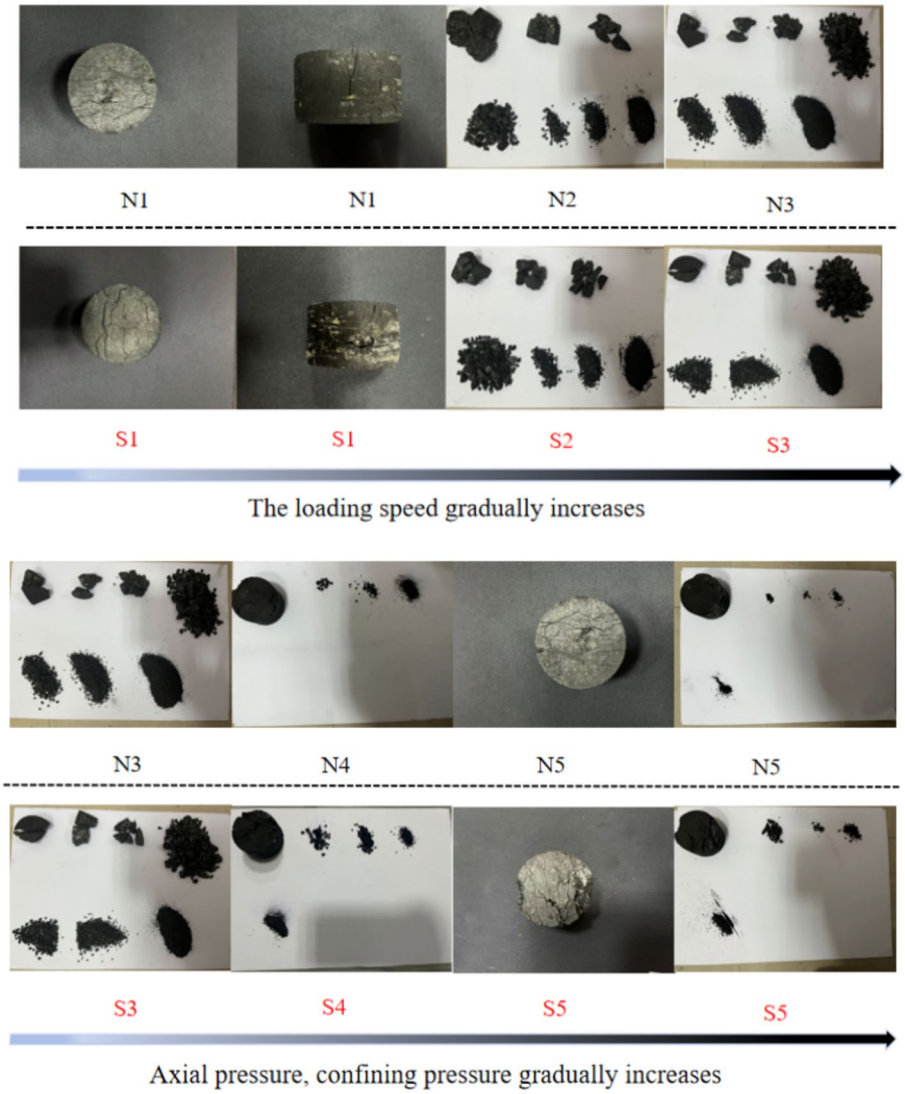

Figure 8. Distribution characteristics of particle size and mass of coal samples under different loading conditions.

Water content	Coal sample number	Sieving diameter/mm						Total mass/g	α	fractal dimension
		30	20	10	3	2	1			
Saturated	S_1	0	0	0	0	0	0	90.33	/	/
	S_2	63.270	48.570	34.820	10.870	7.691	4.151	84.18	0.813	2.187
	S_3	71.360	60.600	51.450	14.450	10.120	4.700	91.09	0.813	2.187
	S_4	4.410	4.410	4.410	3.280	2.300	0.600	86.95	0.470	2.530
	S_5	3.680	3.680	3.680	2.390	1.340	0.410	88.56	0.250	2.750
Natural	N1	0.000	0.000	0.000	0.000	0.000	0.000	86.90	/	/
	N2	46.710	29.230	20.130	6.160	4.250	1.580	89.28	0.950	2.050
	N3	77.580	66.680	55.320	23.420	16.160	7.570	93.61	0.670	2.330
	N4	0.779	0.779	0.779	0.329	0.329	0.109	90.79	0.530	2.470
	N5	2.830	2.830	2.830	0.950	0.810	0.240	91.04	0.690	2.310

Table 4. Fractal analysis of coal sample fragmentation.

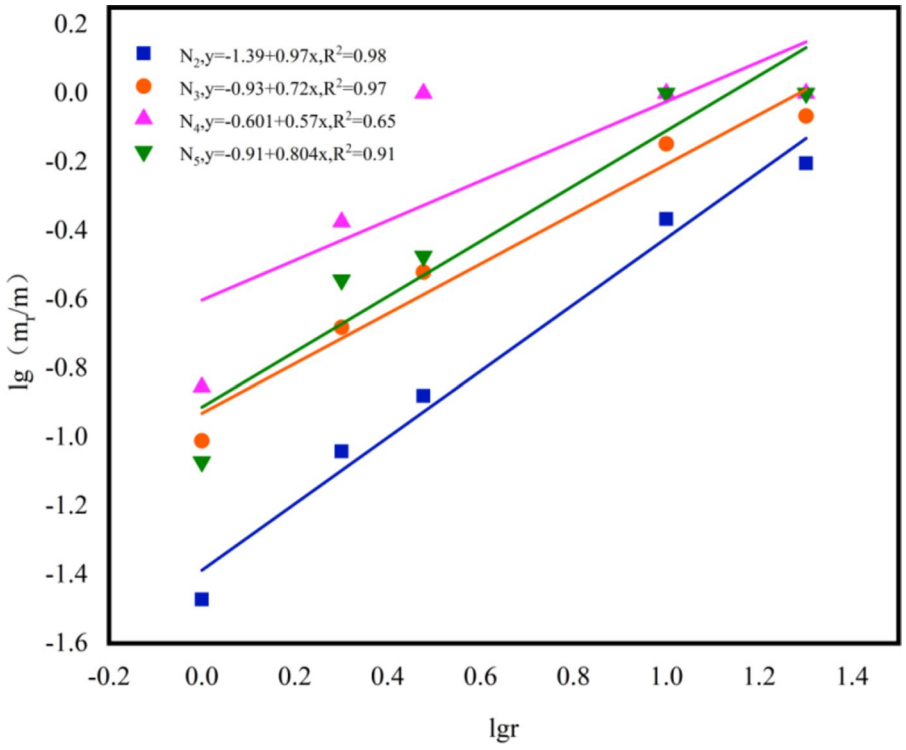

Figure 9. Natural coal sample lg(mr/m) and lgr curves.

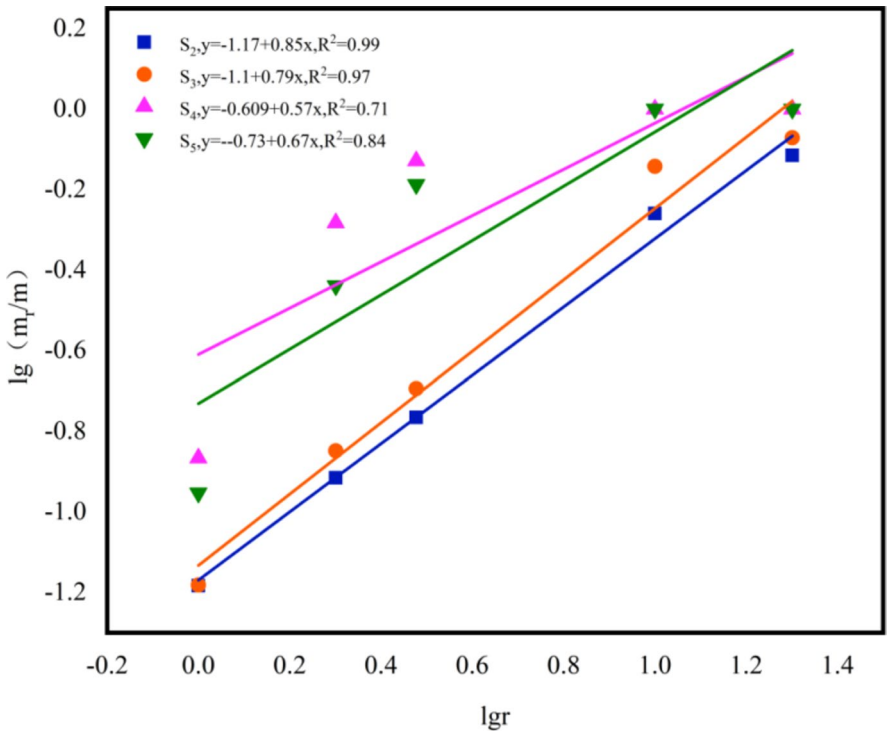

Figure 10. lg(mr/m) and lgr curves of saturated coal samples.

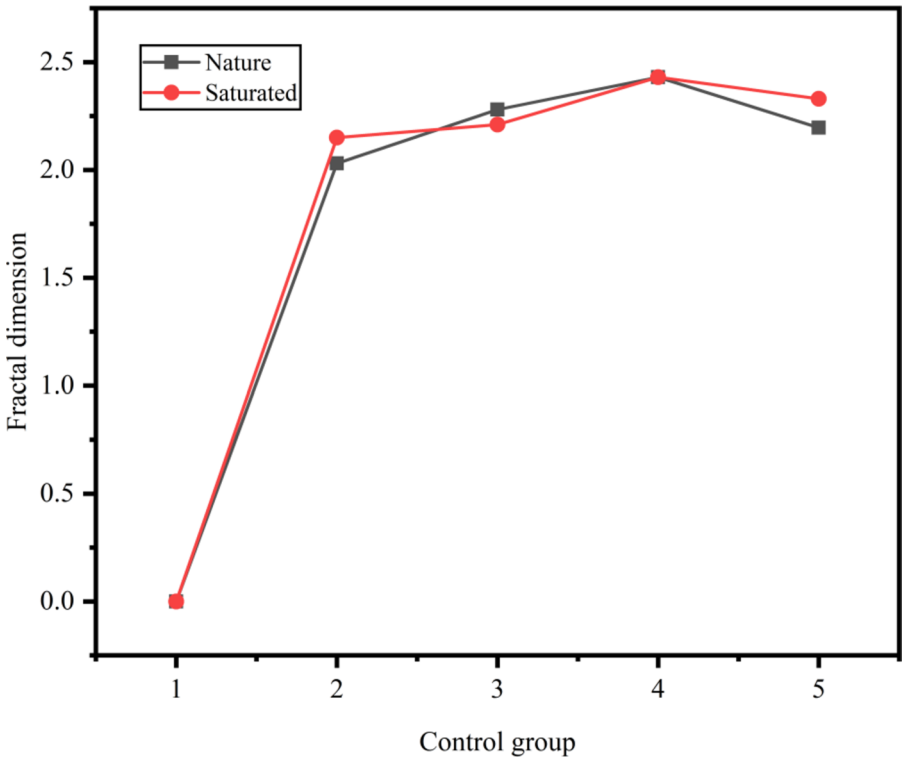

Figure 11. Fractal dimension of natural and saturated coal samples varies with loading rate.

3000 mm; transmission bar, 2500 mm; coal sample, 30 mm; and 50 mm, respectively. These are illustrated in Fig. 12. A numerical simulation analysis was conducted on N1 ~ N4 and S1 ~ S4.

The constitutive model is a macroscopic characterization of the physical and mechanical properties of materials, and is the basis for LS-DYNA material modeling. The HJC model is a computational constitutive model suitable for high strain rate and large strain coal rock media. The HJC model includes 22 parameters in LS-DYNA materials. These parameters are divided into five categories: basic material parameters, material strength parameters, material damage parameters, material pressure parameters, and software parameters. Based on the physical and mechanical properties of the coal and rock used in the experiment, and referring to relevant literature[46], the HJC constitutive model parameters are determined as shown in Table 5, and the basic units of each parameter are in cm-g- μs.

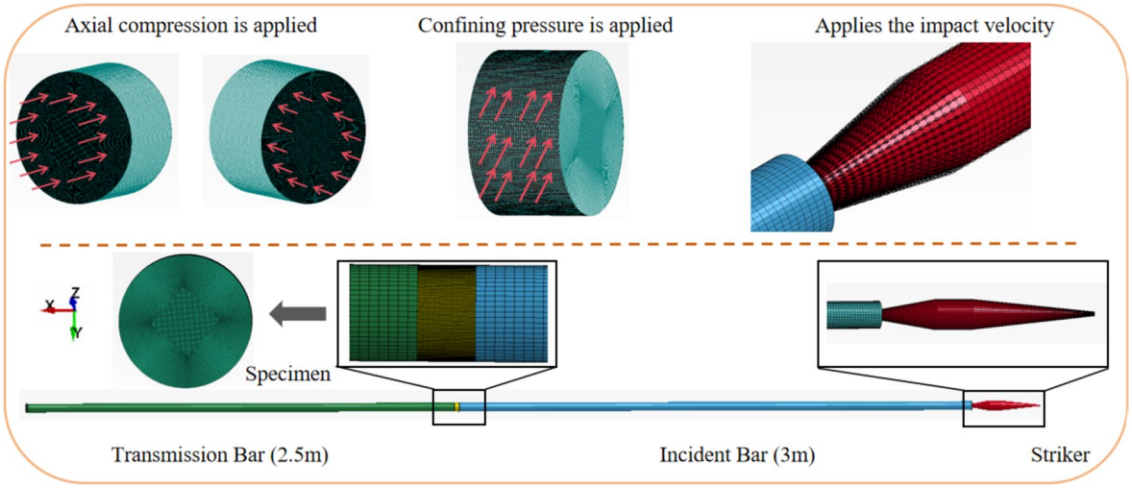

Figure 12. Model schematic.

Parameter	Numerical value	Parametert	Numerical value	Parametert	Numerical value
F_S	0.0	F_C	1.8e-004	P_L	0.008
RO	1.34	T	2.6e-04	U_L	0.109
G	0.01565	EPSO	1.0e-05	D_1	0.032
A	0.59	EF_{MIN}	0.01	D_2	1.00
B	1.9	SF_{MAX}	11.00	K_1	0.0438
C	0.01	P_C	6.0e−05	K_2	0.0607
N	0.92	U_C	7.38e−05	K_3	0.109

Table 5. HJC model parameters.

Numerical simulation results and discussion

In order to verify the accuracy of the numerical simulation and experimental data, a stress uniformity hypothesis test was conducted according to formula (7), where the sum of reflected strain and incident strain is equal to the value of transmitted strain. The three wave diagram of the test results is shown in Fig. 13 (using N1 as an example).

$$\varepsilon_i(t) + \varepsilon_r(t) = \varepsilon_t(t) \tag{7}$$

Figure 13 illustrates that the numerical simulation three-wave diagram has certain similarities with the experimental three-wave diagram. Furthermore, the measured and simulated values are found to be in the same order of magnitude. However, there is still a certain degree of discreteness between the simulation and experimental data. The discrepancy between the simulation and experimental data may be attributed to the transmission accuracy of the experimental equipment. The discreteness of the simulation waveform diagram may be caused by a deviation in the definition of the rod and sample material, but this discreteness is within an acceptable range.

Based on the similarity of the three-wave equilibrium between simulation and experiment, numerical simulations were conducted on the mechanical properties and failure modes of coal samples. In consideration of the weakening effect of water saturation on the mechanical properties of coal samples, the parameters RQ, G, and B in the HJC model were adjusted to 1.24, 0.1465, and 1.6 respectively when simulating saturated coal samples. Figure 14 illustrates that the stress–strain curves of the simulation results are largely congruent with those of the experimental results. Nevertheless, the peak strength enhancement resulting from the combined influence of the bonding force generated by free water and the Stefan effect in the saturated coal sample under high strain rate loading conditions in the experiment was not shown. This is due to the fact that the simulated coal sample has not yet been subjected to microscopic mechanical effects.

Furthermore, the discrepancy between the triaxial mechanical tests and simulation results of natural coal samples and saturated coal samples, as illustrated Fig. 15, indicates that the maximum relative error between the two is calculated and analyzed to be less than 10%. This indicates that the construction of the HJC model can effectively demonstrate the dynamic performance and failure characteristics of coal samples in three-dimensional impact loading tests.

The failure characteristics of coal samples under different loading conditions were obtained through numerical simulation, as shown in Fig. 16. From Fig. 16a, it can be seen that the main failure mode of coal samples is a mixture of shear and tensile failure. Although axial and confining pressures are applied to the coal samples, the energy absorbed by the coal samples from the impact load is relatively concentrated, and the failure starts from the middle of the coal samples. The high axial pressure and confining pressure of the N4 coal sample result in

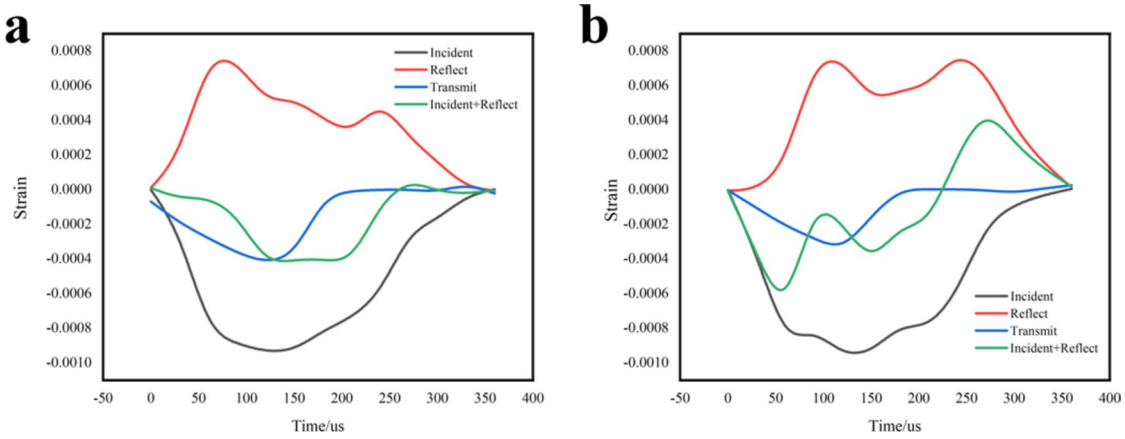

Figure 13. Stress uniformity test (**a**) test, (**b**) simulations.

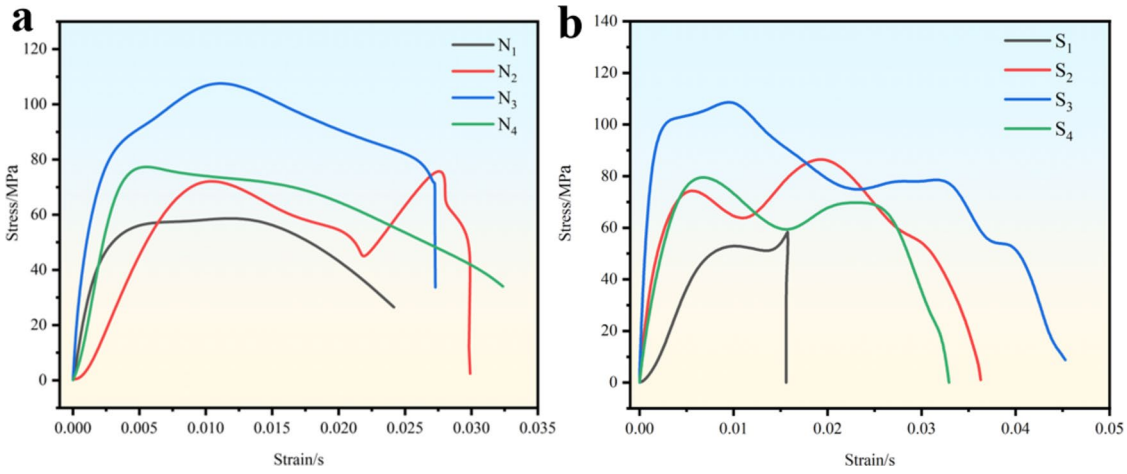

Figure 14. Stress–strain curves of coal samples under different water content states, (**a**) natural coal samples, and (**b**) saturated coal samples.

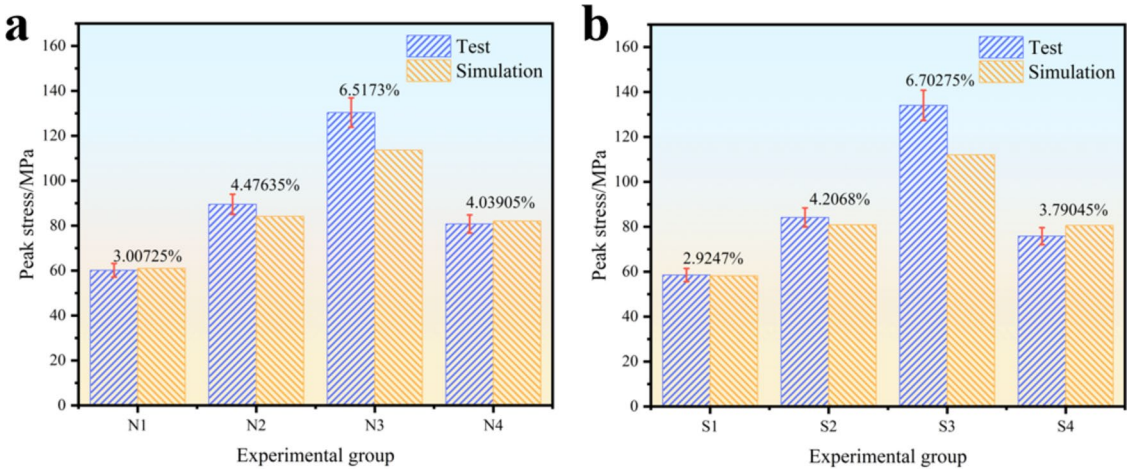

Figure 15. Error analysis of experimental and simulation results.

a reduction in external fragmentation, which in turn leads to a greater degree of ultimate damage to the coal sample. As the strain rate increases, the particle size of coal samples from N1 to N3 becomes smaller, and from 30 stages, it can be seen that the failure mode of coal samples is almost always in an "X" shape from the beginning of failure, which is caused by shear failure. From Fig. 16b, it can be seen that as the strain rate increases, the number of side cracks on the coal sample gradually increases, and the degree of coal sample failure gradually increases. In addition, due to the increase in confining pressure, the number of external cracks in the N4 coal sample becomes more numerous and dense, resulting in a greater degree of coal sample failure.

Discussion on dynamic failure mechanism of saturated coal samples

The failure of coal is caused by the rapid expansion of wing-shaped cracks. However, the promotion of crack propagation is not only related to factors such as strain rate and the physical properties of coal rock itself, but also influenced by the water content state. In the context of static loading conditions, the propagation speed of cracks in the specimen is relatively slow. The influence of surface tension allows the free water present at crack to reach the tip of the crack, where it generates a splitting force on the crack. The generation of pore water pressure is similar to the wedging effect of a "wedge" body, which generates outward compressive stress psw on the wing crack. Concurrently, this process produces a "siphon" effect of free water at the tip of the wing crack, thereby promoting the development or expansion of the crack. The effect of fissure water pressure under static load is shown in Fig. 17a.

In the dynamic loading state, the crack propagation speed is faster than that of free water, which means that the free water in the crack cannot reach the crack tip in a short time. Surface tension pdw is present on the surface of the free water, which is equivalent to the tensile force acting on the crack surface. This hinders the expansion of the crack. As illustrated in Fig. 17b. The surface tension of free water generates an adhesive force, designated F1. Concurrently, the Stefan effect of free water on the crack surface will generate a resistance, F2, that impedes the relative separation of the two crack surfaces[47]. The combined action of F1 and F2 impedes the diffusion of cracks, thereby enhancing the strength of water-bearing coal rock.

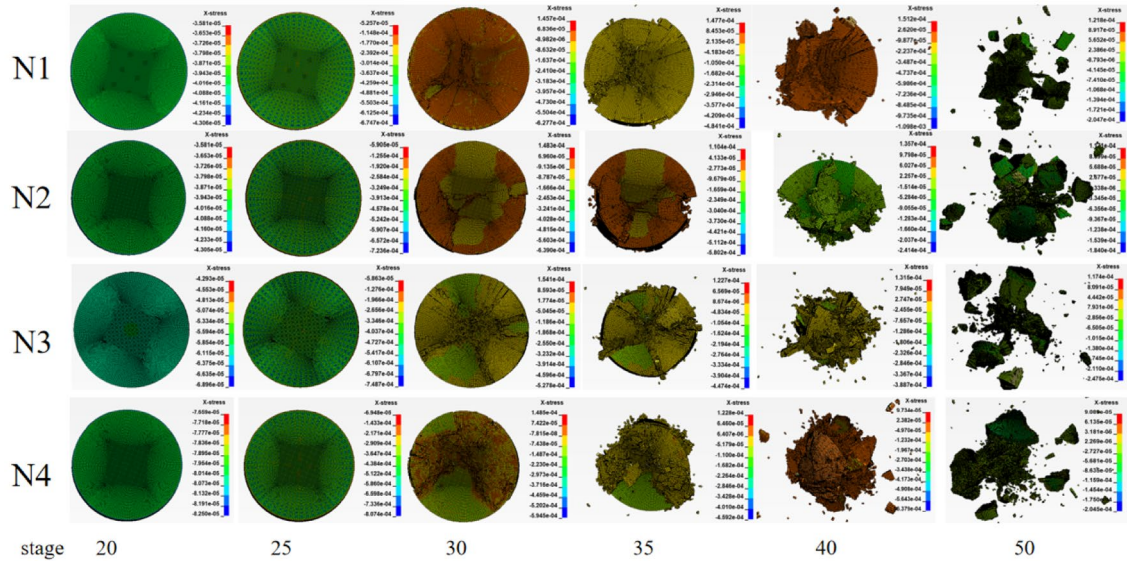

(a) Characteristics of Coal Sample Front Failure

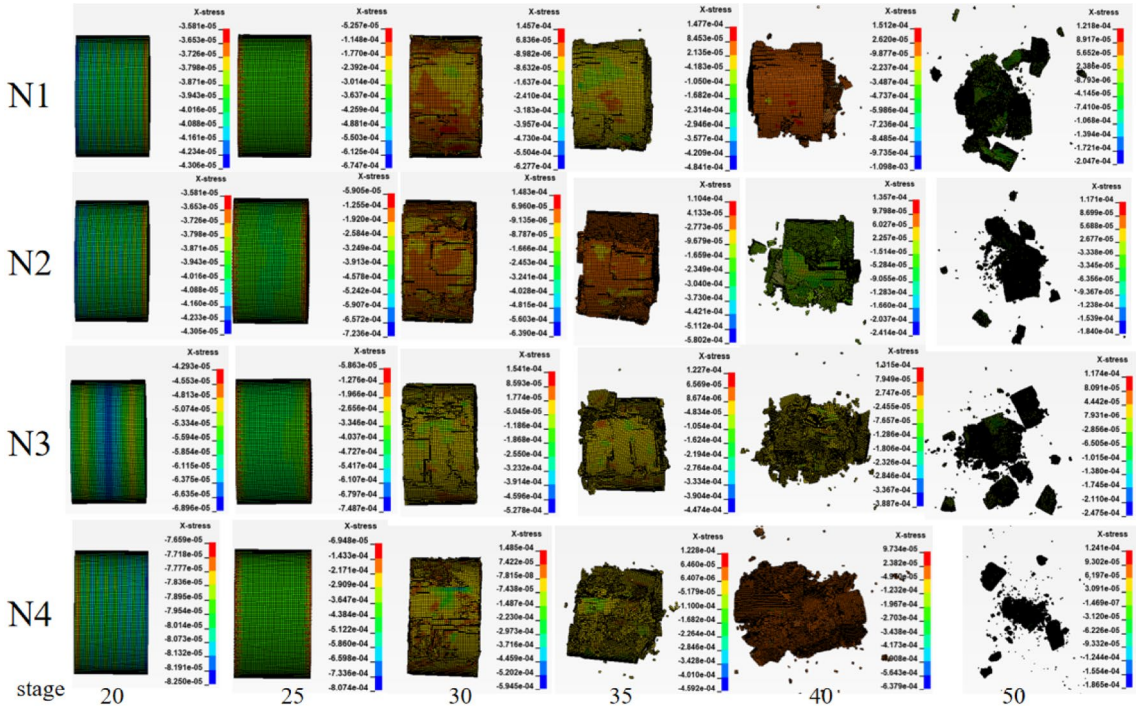

(b) Characteristics of Coal Sample Side Failure

Figure 16. Characteristics of Coal Sample Failure. (**a**) Characteristics of Coal Sample Front Failure, (**b**) Characteristics of Coal Sample Side Failure.

The theoretical analysis of the dynamic failure mechanism of coal rock with water content, as previously discussed, indicates that the water content state of coal rock will alter the original stress field in which the coal rock is situated. In the context of static loading, the outward compressive stress generated by free water at the crack tip serves to promote the development of coal rock cracks, thereby reducing strength and facilitating fragmentation under identical conditions. Conversely, under dynamic loading, free water generates cohesive forces and Stefan effects that impede crack diffusion, resulting in an enhancement of the dynamic strength of coal and rock. This also explains the phenomenon observed in the results of this study, namely that the peak strength of saturated coal samples under high strain rate loading conditions is higher than that in the natural state.

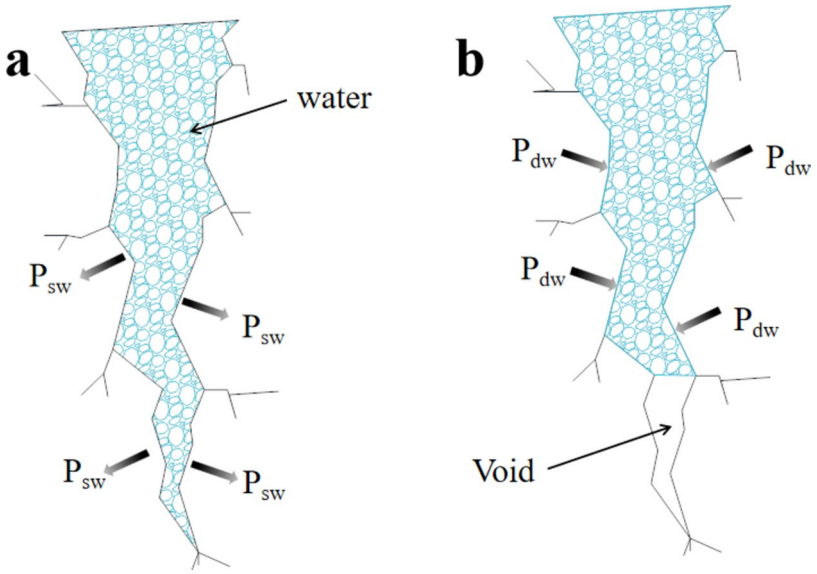

Figure 17. The force of free water on the surface of cracks under dynamic and static loading (**a**) the force of free water on the surface of cracks under static loading conditions (**b**) the force of free water on the surface of cracks under dynamic loading conditions.

Conclusion

To fully understand the effect of saturated water on the dynamic mechanical properties of coal samples, saturated coal samples and natural coal samples were prepared, and the dynamic and static combination loading experiments with different strain rates and different circumferential axial pressures were carried out on coal samples through the SHPB triaxial test system to simulate the force conditions of deep coal rock, and the effects of saturated water on their properties were analyzed, and the main conclusions are as follows:

(1) Under certain strain rate conditions, saturated water has a weakening effect on the dynamic strength of coal samples. When the strain rate is higher than the critical condition, it has a certain enhancing effect on the peak strength of coal samples. Exploring this critical strain rate in engineering practice has certain guiding significance for suppressing rockburst and inducing water injection in coal seams.
(2) The slope α of the curves of natural and saturated coal samples gradually decreases. The fractal dimension gradually increases, and under different confining pressure conditions, the fractal dimension of coal samples decreases with the increase of confining pressure. Under certain strain rate conditions, compared with natural coal samples, the slope α of the saturated coal sample curve gradually decreases at the corresponding loading rate, while the fractal dimension α increases.
(3) As the strain rate gradually increases, the peak strength of saturated coal samples under high strain rate loading conditions is higher than that of natural coal samples under the combined action of bonding force generated by free water and Stefan effect. The numerical simulation based on the HJC model for the triaxial SHPB test can accurately visualize the coal failure process and characteristics, and the experimental and simulation errors are both less than 10%.

Data availability

The datasets used and/or analysed during the current study available from the corresponding author on reasonable request.

Received: 18 May 2024; Accepted: 13 August 2024
Published online: 04 September 2024

References

1. Zhao, Y., Bi, J., Wang, C. & Liu, P. Effect of unloading rate on the mechanical behavior and fracture characteristics of sandstones under complex triaxial stress conditions. *Rock Mech. Rock Eng.* **54**(9), 4851–4866 (2021).
2. Ma, D., Rezania, M., Yu, H. S. & Bai, H. B. Variations of hydraulic properties of granular sandstones during water inrush: Effect of small particle migration. *Eng. Geol.* **217**, 61–70 (2017).
3. Ciantia, M. O., Castellanza, R., Crosta, G. B. & Hueckel, T. Effects of mineral suspension and dissolution on strength and compressibility of soft carbonate rocks. *Eng. Geol.* **184**, 1–18 (2015).
4. He, M., Cheng, T., Qiao, Y. & Li, H. A review of rockburst: Experiments, theories, and simulations. *J. Rock Mech. Geotech. Eng.* **15**(5), 1312–1353 (2023).

5. Li, H. R., Qiao, Y. F., Shen, R. X. & He, M. C. Electromagnetic radiation signal monitoring and multi-fractal analysis during uniaxial compression of water-bearing sandstone. *Measurement* **196**, 111245 (2022).
6. Khosravani, M. R. & Weinberg, K. A review on split Hopkinson bar experiments on the dynamic characterisation of concrete. *Constr. Build. Mater.* **190**, 1264–1283 (2018).
7. Zhang, W., Hao, P., Liu, Y. & Shu, X. Determination of the dynamic response of Q345 steel materials by using SHPB. *Proc. Eng.* **24**, 773–777 (2011).
8. Lok, T. S., Zhao, P. J. & Lu, G. Using the split Hopkinson pressure bar to investigate the dynamic behaviour of SFRC. *Magaz. Concrete Res.* **55**(2), 183–191 (2003).
9. Han, Z., Li, D. & Li, X. Dynamic mechanical properties and wave propagation of composite rock-mortar specimens based on SHPB tests. *Int. J. Min. Sci. Technol.* **32**(4), 793–806 (2022).
10. Chen, X. *et al.* High strain rate compressive strength behavior of cemented paste backfill using split Hopkinson pressure bar. *Int. J. Min. Sci. Technol.* **31**(3), 387–399 (2021).
11. International Society for Rock Mechanics. Commission on Standardization of Laboratory and Field Tests. Committee on Laboratory Tests. *Suggested methods for determining the uniaxial compressive strength and deformability of rock materials*. (1978).
12. Kovari, K., Tisa, A., Einstein, H. H. & Franklin, J. A. Suggested methods for determining the strength of rock materials in triaxial compression: revised version. *Int. J. Rock Mech. Min. Sci. Geomech. Abstr.* **20**(6), 285–290 (1983).
13. Li, X., Zhou, Z., Lok, T. S., Hong, L. & Yin, T. Innovative testing technique of rock subjected to coupled static and dynamic loads. *Int. J. Rock Mech. Min. Sci.* **45**(5), 739–748 (2008).
14. Gong, F. Q., Si, X. F., Li, X. B. & Wang, S. Y. Dynamic triaxial compression tests on sandstone at high strain rates and low confining pressures with split Hopkinson pressure bar. *Int. J. Rock Mech. Min. Sci.* **113**, 211–219 (2019).
15. Yin, T. B., Li, X. B., Gong, F. Q., Zhou, Z. L. & Gao, K. Study of dynamic failure processes and mechanism of rock subjected to coupling temperature and pressure. *Chin. J. Rock Mech. Eng.* **31**(1), 2814–2820 (2012).
16. Zhang, Y., Long, A., Zhao, Y., Zang, A. & Wang, C. Mutual impact of true triaxial stress, borehole orientation and bedding inclination on laboratory hydraulic fracturing of Lushan shale. *J. Rock Mech. Geotech. Eng.* **15**(12), 3131–3147 (2023).
17. Karfakis, M. G. & Akram, M. Effects of chemical solutions on rock fracturing. *Int. J. Rock Mech. Min. Sci. Geomech. Abstr.* **30**(7), 1253–1259 (1993).
18. da Silva, M. R., Schroeder, C. & Verbrugge, J. C. Unsaturated rock mechanics applied to a low-porosity shale. *Eng. Geol.* **97**(1–2), 42–52 (2008).
19. Wasantha, P. L. & Ranjith, P. G. Water-weakening behavior of Hawkesbury sandstone in brittle regime. *Eng. Geol.* **178**, 91–101 (2014).
20. Gu, H., Tao, M., Cao, W., Zhou, J. & Li, X. Dynamic fracture behaviour and evolution mechanism of soft coal with different porosities and water contents. *Theor. Appl. Fract. Mech.* **103**, 102265 (2019).
21. Kim, E., Stine, M. A., de Oliveira, D. B. M. & Changani, H. Correlations between the physical and mechanical properties of sandstones with changes of water content and loading rates. *Int. J. Rock Mech. Min. Sci.* **100**, 255–262 (2017).
22. Kim, E. & Changani, H. Effect of water saturation and loading rate on the mechanical properties of Red and Buff Sandstones. *Int. J. Rock Mech. Min. Sci.* **88**, 23–28 (2016).
23. Mishra, S., Chakraborty, T., Basu, D. & Lam, N. Characterization of sandstone for application in blast analysis of tunnel. *Geotech. Test. J.* **43**(2), 351–382 (2020).
24. Wang, B. *et al.* Split Hopkinson pressure bar (SHPB) experiments on dynamic strength of water-saturated sandstone. *Chin. J. Rock Mech. Eng.* **29**(5), 1003–1009 (2010).
25. Zhou, Z., Cai, X., Cao, W., Li, X. & Xiong, C. Influence of water content on mechanical properties of rock in both saturation and drying processes. *Rock Mech. Rock Eng.* **49**, 3009–3025 (2016).
26. Zhou, Z. L. *et al.* Strength characteristics of dry and saturated rock at different strain rates. *Trans. Nonferrous Metals Soc. China* **26**(7), 1919–1925 (2016).
27. Cai, X., Cheng, C., Zhao, Y., Zhou, Z. & Wang, S. The role of water content in rate dependence of tensile strength of a fine-grained sandstone. *Arch. Civil Mech. Eng.* **22**(1), 58 (2022).
28. Ogata, Y., Jung, W. J., Kubota, S. & Wada, Y. Effect of the strain rate and water saturation for the dynamic tensile strength of rocks. *Mater. Sci. Forum* **465**, 361–366 (2004).
29. Kim, E., Stine, M. A. & Martins de Oliveira, D. B. Effects of water content and loading rate on the mechanical properties of Berea Sandstone. *J. Southern Afr. Inst. Min. Metal.* **119**(12), 1077–1082 (2019).
30. Reviron, N., Reuschlé, T. & Bernard, J. D. The brittle deformation regime of water-saturated siliceous sandstones. *Geophys. J. Int.* **178**(3), 1766–1778 (2009).
31. Wong, L. N. Y., Maruvanchery, V. & Liu, G. Water effects on rock strength and stiffness degradation. *Acta Geotech.* **11**, 713–737 (2016).
32. Liang, X., Tang, S., Tang, C. A., Hu, L. & Chen, F. Influence of water on the mechanical properties and failure behaviors of sandstone under triaxial compression. *Rock Mech. Rock Eng.* **56**(2), 1131–1162 (2023).
33. Serdengecti S, Boozer GD. The effects of strain rate and temperature on the behavior of rocks subjected to triaxial compression. The 4th U.S. Symposium on Rock Mechanics (USRMS), Pennsylvania, pp. 83–97 (1961).
34. Mogi, K. Effect of the triaxial stress system on rock failure. *Rock Mech. Jpn.* **1**, 53–55 (1970).
35. Haimson, B. True triaxial stresses and the brittle fracture of rock. *Pure Appl. Geophys.* **163**, 1101–1130 (2006).
36. Cai, X., Zhou, Z. & Du, X. Water-induced variations in dynamic behavior and failure characteristics of sandstone subjected to simulated geo-stress. *Int. J. Rock Mech. Min. Sci.* **130**, 104339 (2020).
37. Erguler, Z. A. & Ulusay, R. Water-induced variations in mechanical properties of clay-bearing rocks. *Int. J. Rock Mech. Min. Sci.* **46**(2), 355–370 (2009).
38. Cai, M., Hou, P. Y., Zhang, X. W. & Feng, X. T. Post-peak stress–strain curves of brittle hard rocks under axial-strain-controlled loading. *Int. J. Rock Mech. Min. Sci.* **147**, 104921 (2021).
39. Hokka, M. *et al.* Effects of strain rate and confining pressure on the compressive behavior of Kuru granite. *Int. J. Impact Eng.* **91**, 183–193 (2016).
40. Zhao, J. Applicability of Mohr-Coulomb and Hoek-Brown strength criteria to the dynamic strength of brittle rock. *Int. J. Rock Mech. Min. Sci.* **37**(7), 1115–1121 (2000).
41. Lundberg, B. A split Hopkinson bar study of energy absorption in dynamic rock fragmentation. *Int. J. Rock Mech. Min. Sci. Geomech. Abstr.* **13**(6), 187–197 (1976).
42. Colorado-Arango, L., Menéndez-Aguado, J. M. & Osorio-Correa, A. Particle size distribution models for metallurgical coke grinding products. *Metals* **11**(8), 1288 (2021).
43. Vishnoi, N. & Mohapatra, S. K. Study of particle size distribution of pulverized coals in utility boilers. *Part. Sci. Technol.* **36**(8), 999–1005 (2018).
44. Macıas-Garcıa, A., Cuerda-Correa, E. M. & Dıaz-Dıez, M. A. Application of the Rosin-Rammler and Gates–Gaudin–Schuhmann models to the particle size distribution analysis of agglomerated cork. *Mater. Charact.* **52**(2), 159–164 (2004).
45. Grady, D. E. & Kipp, M. E. Geometric statistics and dynamic fragmentation. *J. Appl. Phys.* **58**(3), 1210–1222 (1985).
46. Zhao, S. *et al.* Dynamic mechanical response and crack evolution law of raw coal loaded by dynamic-static coupling under three-dimensional constraints. *Sci. Rep.* **14**(1), 8659 (2024).

47. Zheng, D. & Li, Q. An explanation for rate effect of concrete strength based on fracture toughness including free water viscosity. *Eng. Fract. Mech.* **71**(16–17), 2319–2327 (2004).

Author contributions

Xie Beijing provided overall writing support for the paper, Zhang Ben constructed the overall experimental plan for the paper, Zhao Shunkun conducted computational analysis on the numerical simulation part of the paper, and Wei Shanyang polished and adjusted the overall structure of the paper.

Funding

The work was supported by the State Key Research Development Program of China (Grant No. 2022YFC2904100), the Fundamental Research Funds for the Central Universities (Grant No. 2023ZKPYAQ04) and Guizhou Provincial Key Technology R&D Program (N0.[2023]General Projects 340).

Competing interests

The authors declare no competing interests.

Additional information

Correspondence and requests for materials should be addressed to B.Z.

Reprints and permissions information is available at www.nature.com/reprints.

Publisher's note Springer Nature remains neutral with regard to jurisdictional claims in published maps and institutional affiliations.